Title
Microlattices as architected thin films: Analysis of mechanical properties and high strain elastic recovery

Journal
APL Materials, 1(2)

ISSN
2166532X

Authors
Maloney, Kevin J
Roper, Christopher S
Jacobsen, Alan J
et al.

Publication Date
2013

DOI
10.1063/1.4818168

APL MATERIALS **1**, 022106 (2013)

Microlattices as architected thin films: Analysis of mechanical properties and high strain elastic recovery

Kevin J. Maloney,[1,a] Christopher S. Roper,[1] Alan J. Jacobsen,[1] William B. Carter,[1] Lorenzo Valdevit,[2] and Tobias A. Schaedler[1,b]
[1]*HRL Laboratories LLC, Malibu, California 90265, USA*
[2]*Department of Mechanical and Aerospace Engineering, University of California, Irvine, California 92697, USA*

(Received 1 April 2013; accepted 16 May 2013; published online 13 August 2013)

Ordered periodic microlattices with densities from 0.5 mg/cm^3 to 500 mg/cm^3 are fabricated by depositing various thin film materials (Au, Cu, Ni, SiO_2, poly($C_8H_4F_4$)) onto sacrificial polymer lattice templates. Young's modulus and strength are measured in compression and the density scaling is determined. At low relative densities, recovery from compressive strains of 50% and higher is observed, independent of lattice material. An analytical model is shown to accurately predict the transition between recoverable "pseudo-superelastic" and irrecoverable plastic deformation for all constituent materials. These materials are of interest for energy storage applications, deployable structures, and for acoustic, shock, and vibration damping. [http://dx.doi.org/10.1063/1.4818168]

Cellular materials are created by introducing substantial porosity to a solid material. The effective properties of highly porous materials are determined by the spatial configuration of voids and solid (the "cellular architecture"), as well as the properties of the solid constituent. In contrast to traditional cellular materials (e.g., foams and aerogels), where stochastic methods determine cellular architecture, we study ordered hollow lattices[1] which allow a high degree of control over cellular architecture. Polymer microlattice templates were formed by a unique photopolymerization process which involves an array of intersecting self-propagating waveguides,[3] but could also be fabricated by 3D printing. Several thin film materials were subsequently deposited by a variety of deposition techniques and the solid polymer lattice template was removed by chemical etching.

The fabrication process allows control over three levels of structural hierarchy spanning three orders of magnitude: the hollow tube wall (thickness: ~nm–μm), the hollow tube lattice member (diameter: ~μm–mm), and the lattice unit cell (distance between adjacent lattice members: ~mm–cm).[1] These parameters of the microlattice cellular architecture can be optimized[4] for a given application, e.g., heat exchangers,[5] sandwich panel cores, battery electrodes, catalyst supports, or acoustic, vibration, and shock energy absorbers.[6]

Hollow microlattice samples of varying dimensions were used in this work, most samples having either a truss diameter $D = 400 \pm 50$ μm and a node-to-node distance L = 4 mm, or $D = 100 \pm 20$ μm and $L = 1$ mm. All samples had octahedral cells with a truss angle $\theta = 60^\circ$ and a L/D ratio of ~10 (Fig. 1). Hollow nickel and copper microlattices were manufactured by electroless plating of thin films directly onto the polymer template, which resulted in a nanocrystalline grain structure. Gold was evaporated onto the templates using a rotary planetary fixture in an electron beam evaporator. Thin-film polymer microlattices were fabricated by chemical vapor deposition of poly tetrafluoroparaxylylene (Parylene® AF-4), a fluoropolymer; and silica microlattices were synthesized by atomic layer deposition (ALD) of amorphous silicon dioxide. Properties

[a]Present address: Department of Engineering, University of Cambridge, Cambridge CB2 1PZ, UK
[b]Author to whom correspondence should be addressed. Email: taschaedler@hrl.com

TABLE I. Properties of constituent thin film materials.

Thin film material	Reference	Deposition process	Density g/cm^3	Young's modulus GPa	Yield strength MPa	E_s/ρ_s^2 $\frac{\text{GPa}}{\text{kg}^2/\text{m}^6}$	σ_s/ρ_s^2 $\frac{\text{MPa}}{\text{kg}^2/\text{m}^6}$
Ni-7%P	20	Electroless plating	8.0	210	2500	3.3	39.1
Copper	21	Electroless plating	8.9	119	370	1.5	4.7
Gold	26	Physical vapor deposition	19.3	77	120	0.2	0.3
Silica	26	Atomic layer deposition	2.2	73	1100	15.1	227.3
Parylene	22	Chemical vapor deposition	1.3	2.55	35	1.5	20.7

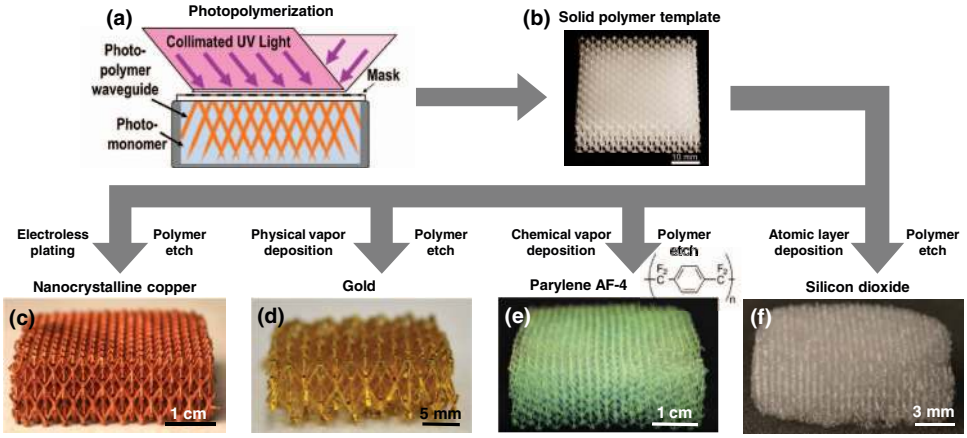

FIG. 1. Fabrication of microlattices from thin film materials. (a) Polymer microlattice templates are synthesized by intersecting self-propagating photopolymer waveguides. (b) The open-cellular, periodic templates can be coated with various thin film deposition techniques and the polymer can be subsequently removed by chemical etching. (c) Copper microlattice by electroless copper plating. (Nickel structures, also fabricated by electroless plating, are not shown.) (d) Gold microlattice by electron beam evaporation. (e) Parylene AF-4 polymer microlattice by chemical vapor deposition. (f) Silicon dioxide microlattice by atomic layer deposition.

of the thin film materials are summarized in Table I. After chemically removing the photopolymer templates, the resulting hollow microlattices were tested in uniaxial compression. The compressive modulus E and compressive collapse strength σ_{pl} are plotted versus density ρ in Fig. 2. Literature data from selected commercially available lightweight materials (closed-cell polymer foams,[7] open-celled polymer foams,[8] aluminum honeycombs,[9] and balsa wood[7]) are shown for comparison. For all hollow microlattices tested in this study, E scales quadratically with ρ, indicating bending-dominated mechanical behavior similar to stochastic, open-celled foams, which exhibit a scaling of[10]:

$$E/E_s \approx C(\rho/\rho_s)^2, \tag{1}$$

where E_s and ρ_s are the Young's modulus and density of the solid constituent material, and the factor C represents the load transfer efficiency of the bending-dominated architecture. Although ordered lattices are expected to exhibit stretching-dominated behavior resulting in linear scaling and superior performance,[11,12] the foam-like scaling of the microlattices under consideration is not surprising. The microlattice architecture is weakened by a lack of truss members in the horizontal plane and by the large voids at the hollow nodes.[2] However, a factor C in Eq. (1) of approximately 3 is determined for all microlattices, which is higher than the typical factor of $C \sim 1$ for foams. This finding is indicative of the superior bending resistance exhibited by a hollow microlattice strut as compared to the bending resistance of solid struts found in open-celled foams.[10] Solving for E in Eq. (1), it is apparent that the material-dependent factor E_s/ρ_s^2 can be used to predict the Young's modulus for microlattices fabricated of a specific material at a given relative density. Empirical data for E is plotted in Fig. 2(a). The ratio E_s/ρ_s^2 is 3.3 for electroless Ni-7%P

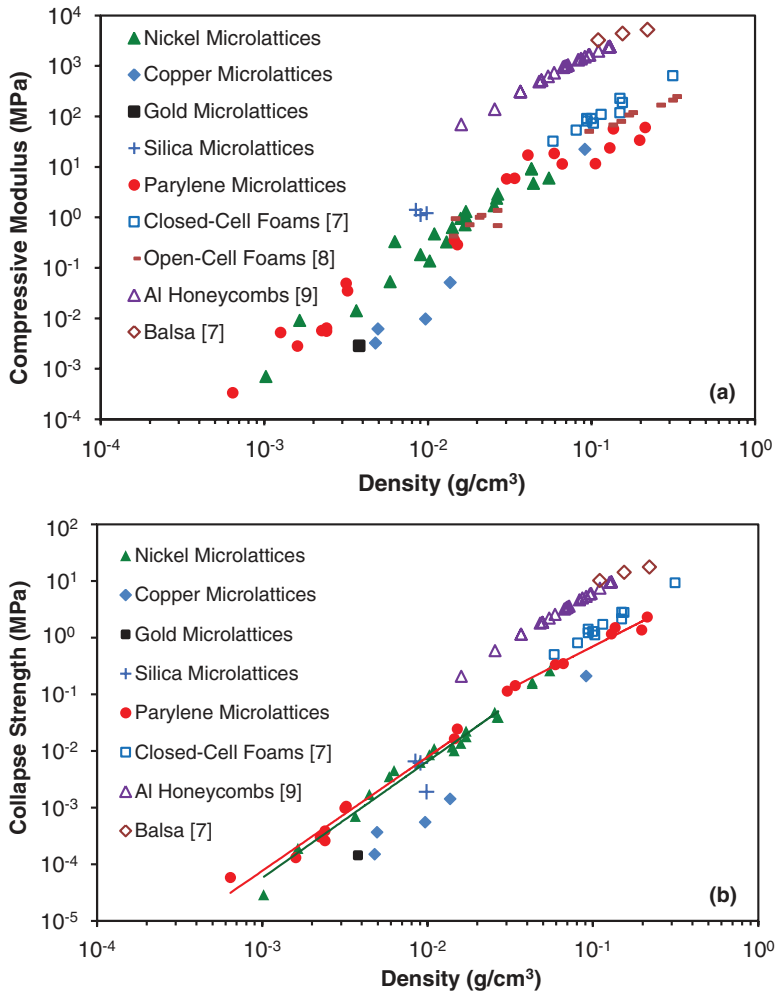

FIG. 2. (a) Compressive modulus and (b) compressive collapse strength vs. density of microlattices fabricated of various materials compared to commercially available lightweight materials.

thin films and 1.5 for parylene (Table I), indicating that nickel microlattices should exhibit a 2× higher modulus than parylene microlattices of the same density, and a slightly smaller difference can be observed when the scattered experimental data are averaged. The ratio $E_s/\rho_s{}^2$ is roughly an order of magnitude lower for gold, and the compressive modulus of a gold microlattice was measured to be in good agreement with the predicted value. Copper exhibits $E_s/\rho_s{}^2 = 1.5$, similar to parylene, but the measured modulus is lower at low densities. This trend is attributed to extensive surface oxidation, which affects the lattice properties more significantly as the film thickness decreases. Amorphous silica has an order of magnitude higher ratio, which is consistent with the experimental results.

The material-independent strength of hollow microlattices is more difficult to distill from experimental data due to competition between multiple failure mechanisms. The compressive strength plotted in Fig. 2(b) is the collapse strength σ_{pl} of the microlattices, which is defined as the maximum stress after yielding (or elastic buckling) and before substantial densification (Fig. 3). Bend-dominated open-celled foams generally fail by yielding, and display a relationship of[10]

$$\sigma_{pl}/\sigma_{y,s} \approx 0.3\left(\rho/\rho_s\right)^{1.5}, \tag{2}$$

where $\sigma_{Y,s}$ is the yield strength of the solid constituent material. Hollow microlattices behave differently in that the failure mode switches from yielding to elastic buckling at a theoretical

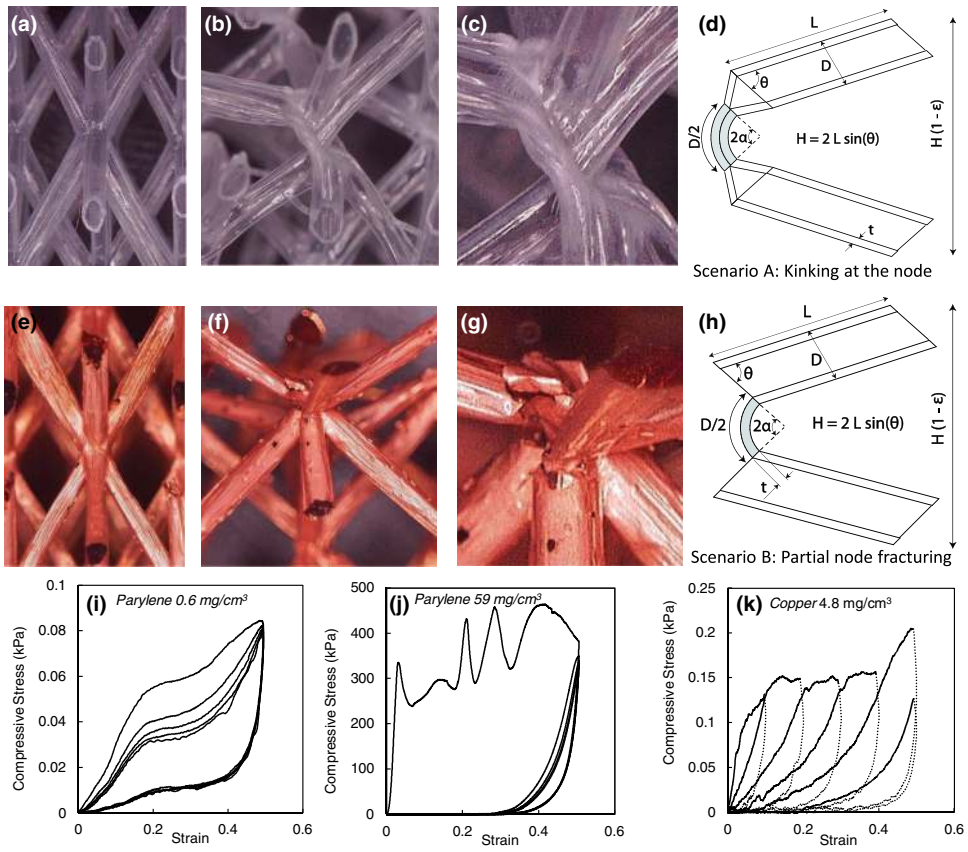

FIG. 3. (a)–(h) Typical deformation modes observed in parylene and copper microlattices and corresponding schematic model. The deformation modes enable large global strain without plastic deformation if the tube wall, t, is small relative to the diameter, D. L/D ~ 10 for all lattices tested. (i) Parylene microlattice with a density $\rho = 0.6$ mg/cm^3, strut diameter D $= 400$ μm, and wall thickness t = 430 nm exhibiting recoverable deformation. (j) Parylene microlattice with $\rho = 59$ mg/cm^3, D $= 400$ μm, and t $= 46$ μm showing 27% residual strain after the first compression. (k) Stress-strain curves for a copper microlattice with $\rho = 4.8$ mg/cm^3, D $= 400$ μm, and t $= 1$ μm tested at increments of 10% strain up to a maximum strain of 50%.

transition density of $0.24\rho_s\sigma_y/E_s$ (for $L/D = 10$ and $\theta = 60^\circ$).[13] For nanocrystalline Ni-7%P, this transition occurs at a density of 0.023 g/cm^3 (Table I), indicating that most of the tested nickel lattices were buckling-limited. The relative strength of the nickel microlattices scales with relative density with an exponent of 2.06 and a pre-exponential constant of 2.5. These values are similar to a previous assessment of a subset of these samples[2] and agree with observed behavior. Deformation is dominated by local elastic buckling and brittle fracture at the nodes, therefore the samples are weaker (scaling > 1.5) than predicted by the plasticity-based model in Eq. (2).

As parylene has a much lower yield strength than nickel, parylene microlattices should remain yielding-limited down to a density of ~0.0043 g/cm^3. The observed transition is at a density of ~0.02 g/cm^3. A scaling of $\sigma_{pl}/\sigma_y = 0.9\left(\rho/\rho_s\right)^{1.49}$ is measured above and a scaling of $\sigma_{pl}/\sigma_y = 4.2\left(\rho/\rho_s\right)^{2.01}$ is measured below this density. The disagreement on the transition density is attributed to local deformation of the hollow nodes (not captured in analytical beam-theory models).

Finite element calculations based on geometrically accurate models of the hollow nodes are currently being developed to confirm this interpretation; additionally, these calculations will shed light on the specific deformation mechanisms of thin-walled hollow lattices made of a number of materials.[13] Comparing the strength scaling of microlattices formed from parylene polymer and nanocrystalline Ni-7%P (which behaves more like a brittle metallic glass than a ductile metal)

demonstrates that cellular architecture has as much impact on the mechanical performance of microlattices as the constituent material properties. For the copper, gold, and silica microlattices, no conclusions about the trends of strength vs. density can be drawn from the limited experimental data, which fall close to the transition densities. The nanocrystalline copper and silica samples failed by buckling and brittle fracture; gold microlattices showed extensive buckling and kinking but little fracture. The order-of-magnitude lower strength of the nanocrystalline copper microlattices as compared to Ni-7%P is consistent with the 8.4× lower ratio $\sigma_y/{\rho_s}^2$, the material-dependent scaling factor in the low-density regime. Silica shows a 5.8× higher $\sigma_y/{\rho_s}^2$ ratio than Ni-7%P, but the strength of the measured samples was similar or lower than Ni-7%P, presumably due to the much lower failure strength ($\sim 0.1\sigma_y$) dictated by the low fracture toughness of glass.

High-strain recoverability, reported previously in carbon nanotube forests[14–16] and viscoelastic polymer foams,[10] is observed in thin-film microlattices across multiple materials. At higher relative densities, this recoverability disappears and plastic deformation typical of regular metallic cellular materials or brittle fracture typical of a ceramic foam is observed. Compressive stress-strain curves for two parylene samples with identical dimensions $L = 4$ mm, $D = 0.4$ mm, and $\theta = 60^o$ but different wall thicknesses ($t = 430 \pm 100$ nm and $t = 46 \pm 1$ μm) are shown in Figs. 3(i) and 3(j). While the thin-walled microlattice displays complete recovery from 50% strain after multiple compression cycles, the thick-walled microlattice displays large plastic deformation and 25% residual strain after the first compression to 50% strain. (The irregular stress-strain response of the microlattice in Fig. 3(j) is caused by the sequential buckling of distinct layers.) Similar behavior is observed in nickel,[2] copper, gold, and silica microlattices. A transition between recoverable and irrecoverable deformation was observed in a copper microlattice sample (Fig. 3(k)) tested at increments of 10% strain up to a maximum compressive strain of 50%. After 30% strain, the copper sample displayed a residual strain of only 6%; when compressed to a strain of 50%, residual strain increased to 18%.

A model has been developed which predicts the ratio of wall thickness t to strut diameter D at the transition between recoverable elastic and irrecoverable plastic deformation.[2] The model assumes that large strains in microlattices are enabled by rotation of the bars about thin ligaments in the proximity of the nodes, generated either by kinking (local buckling) or partial node fracture (Fig. 3). As the ligaments have thicknesses similar to the bar wall thickness (in the 100 nm–50 μm range), large rotations are possible without introducing plastic strains. The critical wall thickness at which plastic deformation would commence can be expressed as

$$\left(\frac{t}{D}\right)_{cr} = \frac{\sigma_{Y,s}}{E_s} \frac{0.25}{\theta - \sin^{-1}[(1-\varepsilon_{max})\sin\theta]}, \tag{3}$$

where ε_{max} is the maximum global strain the microlattice experiences, and θ is the truss angle in radians.

Figure 3 explores the two deformation mechanisms by comparing deformation of parylene and copper microlattices. The deformation starts at the nodes and the nodes play a critical role in how the deformation continues. A node of a parylene microlattice is shown in Fig. 3(a), while Fig. 3(b) shows this node after the lattice has been compressed by approximately 50%. Kinking and bending is observed but the parylene thin film does not fracture. Large strain is known to induce crystallization in polymers, creating micron-size grains that scatter light much more efficiently than the amorphous polymer material (also referred to as crazing[17]). Localized deformation of the bulk parylene is indicated by small areas of white discoloration in a close-up picture of the node (Fig. 3(c)), but most of the deformed parylene stays clear, demonstrating that the lattice withstands large strain by kinking at the node and bending. By contrast, the copper lattice fractures at the node, while the struts stay intact (Figs. 3(f) and 3(g)). The struts do not fracture completely and the remaining ligaments can bend and withstand large global strain. The schematics for the deformation modes in Figs. 3(d) and 3(h) are simplified to enable calculation of the critical ratio of wall thickness to lattice member diameter for the transition between recoverable elastic and irrecoverable plastic deformations (Eq. (3)).[2] Nanocrystalline copper and silica microlattices display partial node fracture: the same deformation mechanism previously observed in nanocrystalline nickel microlattices.[1,2]

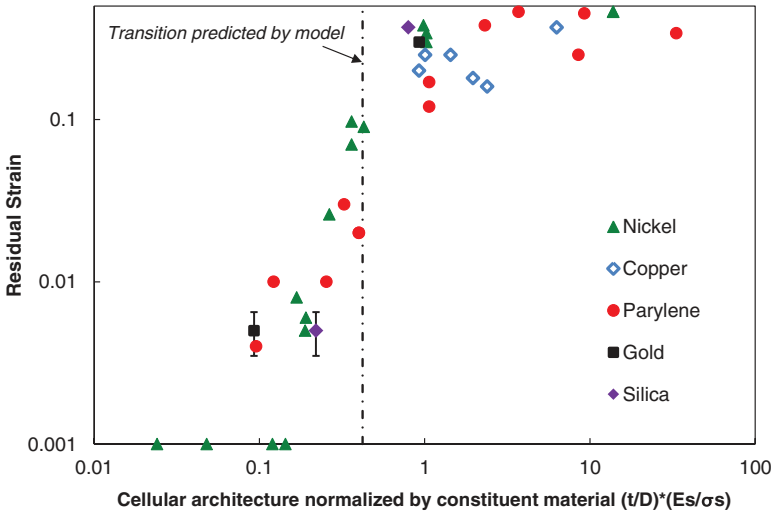

FIG. 4. Residual strain after ~50% compression of hollow microlattices fabricated from different materials plotted against cellular architecture (tube wall thickness/diameter) and constituent material parameters. The dashed line is the predicted transition between recoverable elastic deformation and irrecoverable plastic deformation according to Eq. (3).

Parylene and gold microlattices display kinking and bending at the nodes to enable large global strain without any node fracture.

Residual strain data extracted from compressive stress-strain plots are plotted in Fig. 4 versus the product of thickness to diameter ratio and constituent modulus to yield strength ratio $(t/D)^*(E_s/\sigma_{y,s})$. The dotted line indicates the material-independent predicted critical wall thickness-to-diameter ratio $(E_s/\sigma_{y,s})^*(t/D)_{cr}$ and is shown to agree well with the experimentally observed transition between recoverable elastic and irrecoverable plastic deformations across all tested materials. Equation (3) is shown to accurately predict $(t/D)_{cr}$ for both of these deformation mechanisms, indicating that the architecture of the cellular material dominates the load response although the constituent materials behave fundamentally differently.

Although a grain rotation mechanism has recently been shown to be responsible for large reversible strains in freestanding aluminum thin films,[18] the good correlation of the analytical model with microlattices of different materials indicates that classical elastic deformation is responsible for the surprising "springiness" of these microlattices.

This work deepens the understanding of the roles of cellular architecture and constituent material properties on the stiffness and strength (as well as the transition between recoverable elastic deformation and irrecoverable plastic deformation) of hollow microlattices, thus enabling design of microlattices with tailored properties for specific applications. This work also demonstrates that microlattices can be fabricated from a wide variety of metals, polymers, and ceramics using different thin film deposition methods. In principal, any thin film material can be converted into a three-dimensional lattice material with this approach provided there is a non-line-of-sight process, sufficient etch selectivity, and film cohesion, offering an exciting expansion of available cellular materials. Materials that recover quickly after large strains are of interest for energy storage applications, which involve the expansion of a substrate material after intercalation or adsorption, and for deployable structures that need to be stowed at reduced volume (e.g., during launch into space) and then expand to normal size. Since microlattice materials absorb energy on compression and recovery, they are also of interest for acoustic, shock, and vibration damping.

Thiol-ene microlattices were fabricated from an interconnected pattern of self-propagating photopolymer waveguides as described in detail in Refs. 3 and 19. After postcuring at 120 °C in air for 12 h, the polymer microlattices were used as direct templates for deposition of thin films. Nickel and copper were deposited by electroless plating using a commercially available process (OM Group Inc., Cleveland, OH), which resulted in a nanocrystalline microstructure of nickel with

7 wt.% phosphorous with a grain size of 7 nm[20] and pure copper with a grain size of ∼10 nm, respectively,[21] see Ref. 1 for details. Parylene AF4, a fluorinated poly(p-xylylene) polymer (see Fig. 1) was deposited by chemical vapor deposition by Specialty Coating Systems™, Inc. Di-para-xylylene dimer was vaporized at 150 °C and 1 Torr, pyrolyzed to the monomer at 600 °C and 0.5 Torr and then deposited as polymer at 25 °C and 0.1 Torr.[22,23]

Silica was deposited as an amorphous thin film by ALD by Arradiance Inc. in Sudbury, Massachusetts. Tris(*tert*-butoxy)silanol precursor was used at a temperature of 95 °C and deposited at 150 °C in a GEMStar® system with the catalysis of trimethylaluminum, which resulted in a fast growth rate of approximately 10 nm/cycle comparable to reports in the literature.[24,25]

Gold was deposited as crystalline thin film by electron beam evaporation using a CHA Industries Mark 50 electron beam evaporator. A rotary, 3-dome planetary fixture was used to continuously change the microlattice's angle with respect to the evaporant stream, and the microlattice was flipped over halfway through the deposition to improve coverage. By selecting a microlattice with less cells across the thickness and a more open structure (Fig. 1) non-uniformities in the gold film thickness could be minimized.

After deposition of the different thin films, the top and bottom surfaces of each microlattice were sanded to expose the underlying polymer. The polymer was then chemically etched in a base solution (1.5M NaOH in 50% H_2O/50% methanol at 60 °C), creating the hollow microlattices shown in Fig. 1. The lightest samples were freeze dried after exchanging the NaOH solution to deionized water and then to t-butanol in order to avoid collapse on removal from solution. The film thickness was measured by cross-sectional scanning electron microscopy (SEM) and verified by comparing measured densities with a computer aided design (CAD) model.

The compression tests were performed on a servo-electric INSTRON® 5565 frame. The displacement rate was 0.01 mm/s for loading and unloading, and microlattices of similar dimensions as shown in Fig. 1 were tested between compression platens without attachment. The loads were measured by a SENSOTEC® load cell with a range of 250 N or an INSTRON load cell with a range of 500 N, and the displacements were measured by an Electronic Instrument Research laser extensometer (Ref. 26).

This investigation was sponsored by the Defense Advanced Research Projects Agency under the Materials with Controlled Microstructural Architecture program managed by J. Goldwasser (Contract No. W91CRB-10-0305). The authors would like to thank A. Sorensen and M. Allenby (HRL Laboratories, LLC) for help with sample preparation and testing.

[1] T. A. Schaedler, A. J. Jacobsen, A. Torrents, A. E. Sorensen, J. Lian, J. R. Greer, L. Valdevit, and W. B. Carter, Science **334**, 962–965 (2011).
[2] A. Torrents, T. A. Schaedler, A. J. Jacobsen, W. B. Carter, and L. Valdevit, Acta Mater. **60**, 3511–3523 (2012).
[3] A. J. Jacobsen, W. B. Carter, and S. Nutt, Adv. Mater. **19**, 3892–3896 (2007).
[4] C. S. Roper, Int. J. Heat Fluid Flow **32**(1), 239–248 (2011).
[5] K. J. Maloney, K. D. Fink, T. A. Schaedler, J. A. Kolodziejska, A. J. Jacobsen, and C. S. Roper, Int. J. Heat Mass Transfer **55**, 2486–2493 (2012).
[6] A. G. Evans, M. Y. He, V. S. Deshpande, J. W. Hutchinson, A. J. Jacobsen, and W. B. Carter, Int. J. Impact Eng. **37**, 947–959 (2010).
[7] A. G. Gurit Holding, Core-Cell Datasheets, see http://www.gurit.com/core-materials-datasheets.aspx and http://www.gurit.com/files/documents/balsaflexwev3pdf.pdf.
[8] L. J. Gibson and M. F. Ashby, Proc. R. Soc. London, Ser. A **382**, 43–59 (1982).
[9] Plascore Inc. PAMG-XR1 5052 Aluminum Honeycomb, Datasheet, 2012, see http://www.plascore.com/pdf/Plascore_5052.pdf.
[10] L. J. Gibson and M. F. Ashby, *Cellular Solids: Structure and Properties* (Cambridge University Press, 1997).
[11] V. S. Deshpande, N. A. Fleck, and M. F. Ashby, J. Mech. Phys. Solids **49**, 1747 (2001).
[12] A. G. Evans, J. W. Hutchinson, N. A. Fleck, M. F. Ashby, and H. N. G. Wadley, Prog. Mater. Sci. **46**, 309 (2001).
[13] L. Valdevit, S. W. Godfrey, T. A. Schaedler, A. J. Jacobson, and W. B. Carter, "Compressive strength of hollow microlattices: Experimental characterization, modeling, and optimal design," J. Mater. Res. (published online).
[14] J. Zou, J. Liu, A. S. Karakoti, A. Kumar, D. Joung, Q. Li, S. I. Khondaker, S. Seal, and L. Zhai, ACS Nano **4**, 7293–7302 (2010).
[15] M. Xu, D. N. Futaba, T. Yamada, M. Yumura, and K. Hata, Science **330**, 1364 (2010).
[16] S. B. Hutchens, A. Needleman, and J. R. Greer, J. Mech. Phys. Solids **59**, 2227–2237 (2011).
[17] E. J. Kramer, Adv. Polym. Sci. **52–53**, 1–56 (1983).
[18] S. Kumar, M. T. Alam, and M. A. Haque, J. Microelectromech. Syst. **20**(1), 53 (2011).

[19] A. J. Jacobsen, W. B. Carter, and S. Nutt, Acta Mater. **55**, 6724–6733 (2007).
[20] J. Lian, L. Valdevit, T. A. Schaedler, A. J. Jacobsen, W. Barvosa-Carter, and J. R. Greer, Nano Lett. **11**, 4118 (2011).
[21] S.-Y. Chang and T.-K. Chang, J. Appl. Phys. **101**, 033507 (2007).
[22] J. J. Licari, *Coating Materials for Electronic Applications* (Noyes Publications, 2003).
[23] *Handbook of Plastics, Elastomers and Composites* (McGraw Hill, Inc., 2002), Chap. 6.
[24] D. Hausmann, J. Becker, S. Wang, and R. G. Gordon, Science **298**, 402–406 (2002).
[25] B. B. Burton, M. P. Boleslawski, A. T. Desombre, and S. M. George, Chem. Mater. **20**, 7031–7043 (2008).
[26] W. D. Callister, *Materials Science and Engineering: An Introduction* (John Wiley and Sons, Inc., 2000).